DESIGNED BINARY MIXTURES FOR SUBCRITICAL ORGANIC RANKINE CYCLES BASED ON MULTIOBJECTIVE OPTIMIZATION

C. J. Noriega Sanchez[1], Louis Gosselin[2] and Alexandre K. da Silva[1]

[1] Department of Mechanical Engineering, Federal University of Santa Catarina, Florianopolis, SC, 88040-900, Brazil

[2]Department of Mechanical Engineering, Université Laval, Quebec City, QC, Canada

Article accepté pour publication dans : Energy Conversion and Management, Volume 156, 15 janvier 2018

Abstract

The use of binary zeotropic mixtures as working fluids applied to Organic Rankine Cycles (ORCs) is investigated in this paper. In total, six (6) hydrocarbons and (2) hydrofluorocarbons are considered, leading to twenty-eight (28) possible binary combinations. The mixtures were tested with a basic Rankine cycle while using the heat source temperature as independent variable, which assumed six different values, ranging from 80°C to 180°C, in steps of 20°C. The simulations aimed to identify the ideal mixtures that maximized the net power and exergetic efficiency, and minimized the heat exchanger's global conductance for a given temperature of the heat source. The optimization process relied on a genetic algorithm and the selection of the best mixtures, on a non-dominated sorting method (NDS), which returned Pareto fronts gathering the best solutions. While no one specific ideal mixture was identified, the results showed that the range of the so-called ideal mixtures narrows as the heat source temperature increases, with mixtures including fluids like R245fa and pentane being good options, whereas at low temperature, a larger number of fluid mixtures perform well. Finally, a scale analysis is proposed and shows that maximal net power varies linearly with a Number of Transfer Units (NTU) factor while its slope depends on the heat source temperature. The latter analysis is compared with the results obtained with the Pareto front and NDS, showing that both sets of results agree well while correlated by a single constant for the entire temperature range covered in the present study.

Keywords: Organic Rankine Cycle (ORC); Working fluid; Mixture; Genetic algorithms (GA); Multi-objective optimization.

Nomenclature

$\dot{I}$	Flow rate of exergy destruction, kW
h	Enthalpy, kJ/kg
h_{fg}	Latent heat of evaporation, kJ/kg
$\dot{m}$	mass flow, kg/s
P	Pressure, kPa
s	Entropy, kJ/kg.K
T	Temperature, °C
(UA)	Global conductance, kW/K
x	Quality

Greek Symbols

η	Efficiency
Δ	Difference
ϕ	Mass fraction

Subscripts

0	Dead state
C	Cold
Co	Condenser
Crit	Critical
Eva	Evaporator
Exe	Exergy
G	Generator
hs	Heat source

H	Hot
is	Isentropic
L	Low
mix	Mixture
M	Mechanic
P	Pump
cs	Cold source
T	Turbine
wf	Working fluid

Acronyms

GA	Genetic Algorithm
GWP	Global Warming Potential
HFC	Hydrofluorocarbon
HC	Hydrocarbon
NDS	Non-Dominated-Solutions
NTU	Number of transfer units
ODP	Ozone Depletion Potential

1. Introduction

Modulability, lower costs and higher efficiency are some of the advantages that Organic Rankine Cycles (ORC) offer while producing power from medium and low temperature heat sources [1]. Nevertheless, current heat-to-electricity conversion efficiency is still relatively low with such cycles, i.e. around 10% [2]. Recent research has focused on improving the performance of ORCs through the study and optimization of ORC configurations, expansion devices and suitable working fluids, among others [3].

For instance, the optimal working fluid highly depends not only on the conditions for which the cycle is designed (e.g., temperatures of heat source and of heat sink), but also on the criteria that are used to evaluate the cycle's performance (e.g., net power output, exergy efficiency, equipment size, overall cost, environmental footprint, etc.). In this regard, the working fluid choice is one of the most critical design parameters, and identifying the "best" fluid is far from trivial.

In the literature, several studies have aimed at identifying suitable working fluids for ORC applications. Recently, Habibzadeh and Rashidi investigated 13 different working fluids in ORCs, and found that R141b, R123 and R717 were the best isentropic, dry and wet working fluids respectively [4]. Chagnon-Lessard et al. determined the best working fluid in ORCs among a list of 36 as a function of the heat source and condenser's temperatures while considering a single objective function, namely the specific power output, and only pure fluids were studied [5]. Optimal selection of working fluid from a list of 26 fluids was also proposed in Ref. [6]. It was found that the optimal working fluids (i.e. the ones leading to the maximal power output) typically had a critical temperature ~30-50 K above the heat source temperature.

Zeotropic mixtures have been receiving more and more attention over the last years as potential working fluids for ORC [7–12]. Indeed, in some applications, mixtures can be more suitable than pure working fluids because they allow a better temperature matching during the heat transfer processes, which decreases the irreversibilities and increases the system's efficiency and net power [13]. This is mainly due to the phase transition of mixtures, which is isobaric but not isothermal [7].

Chys et al. evaluated the heat recovery potential of 12 pure organic fluids as well as their binary and ternary mixtures considering heat source temperatures of 150°C and

250°C [9]. The authors determined the optimal concentration in order to produce the maximum power output. The results showed that zeotropic mixtures had a positive effect on the system's performance and electric energy production, especially with the 150°C heat source. However, the inclusion of a third component in the mix only had a marginal impact on the cycle performance. A comparison between a few mixtures and pure fluids was also performed in Ref. [14]. First law and second law efficiencies were studied. Better thermal performance was achieved when the temperature difference of the cooling water was near the temperature glide of the mixture in the condenser. Moreover, Braimakis et al. found that the substitution of pure fluids by hydrocarbons binary mixtures has the potential to increase the cycle exergy efficiency for both subcritical and transcritical conditions with heat source temperatures between 150°C and 300°C [15].

One of the advantages that fluid mixtures offer is the possibility to finely tune the fluid composition to the context for which the ORC is being designed. The idea of dynamic ORCs in which the fluid composition could change in time depending on the operating conditions was proposed in Ref. [16]. A systematic approach was also developed in Ref. [12] for a fast evaluation of large sets of fluids and mixtures. The authors found that for the temperature level considered in their study (138°C), a mixture of R365mfc/R1234yf led to 10% more power and similar efficiency without wet expansion in the turbine when compared with the best pure fluid (R1234ze) with wet expansion.

The potential of zeotropic blends has also been addressed through multi-objective studies. In Ref. [17], ten defined zeotropic mixtures and R245fa as a pure working fluid were evaluated for three ORC configurations using geothermal water as the heat source. The net power output and TSP (turbine size parameter) were the two objective functions. The results showed that the use of zeotropic mixtures leads to more power generation in all configurations and lower values of TSP as well. The fluid composition was not optimized explicitly in that work. Feng et al. performed a multi-objective optimization of ORCs based on exergy efficiency and levelized energy cost [18]. Pure fluids and mixtures were compared as potential working fluids. Although only one type of mixtures was considered, it was found that mixtures typically had better exergy efficiency but worse levelized energy cost compared to pure fluids. Additionally, a multi-objective cost-power optimization for low temperature heat sources was done in Ref. [19]. The results indicated

that working fluid mixtures show a thermodynamic improvement over the pure-fluids, but are also associated with higher costs.

Despite extensive research efforts over the last years to optimize ORC designs, and in particular to select optimal working fluids, there is still a lack of general design tools and guidelines for working fluid selection, in particular for fluid mixtures. Therefore, the objective of this article is to find suitable working fluid mixtures for typical heat source levels founded in ORC applications, considering three objective functions at the same time (multi-objective optimization). Two objectives are related to the system performance, i.e., net power output $\dot{W}_{Net}$ and exergy efficiency η_{Exe}, and the third objective function is the global conductance $(UA)_{Total}$ as an indication of the size of the system [20, 21]. Different heat source temperature levels are investigated for a series of twenty-eight (28) working fluid binary mixtures, involving HCs and HFCs. The paper is divided as follows: Section 2 describes the thermodynamic model of the power cycle and the working fluids studied in this work. The multi-objective optimization problem and the approach used to solve it are presented in Section 3. The results and discussion follow in Section 4 while a scale analysis is proposed in Section 5.

2. Methodology

2.1 Heat source

Hot combustion gases are among the most common waste heat source in industrial installations. However, when these are used directly in heat recovery applications, potential corrosion problems can limit the minimum heat exchanger output temperature. Furthermore, recovering heat from gases requires large heat transfer areas because of the limited heat transfer coefficient of gases, which dominates the global heat transfer coefficient. In the present work, the heat source fluid was thus considered to be pressurized water. This choice eliminates the above-mentioned issues. Also, it applies to different power plants, such as those relying on geothermal heat. The inlet heat source pressure was assumed to be 1000 kPa in such a way that the heat source temperature could vary from 80°C to 180°C. In this work, considering increments of 20°C, a total of six heat source temperatures were analyzed. The other characteristics of the heat source are presented in Table 1. Note that a mass flow rate of 1 kg/s was used since the power output, working

fluid mass flow rate, etc., were expressed per unit of the heat source fluid flow rate. In other words, the power output reported is actually the specific power.

Table 1. Characteristics of heat source in this work.

Variable	Symbol	Value or Range
Heat source mass flow	$\dot{m}_{hs}$	1 kg s^{-1}
Hot fluid inlet temperature	$T_{hs,in}$	80 – 180 °C
Heat source pressure	$P_{hs,in}$	1000 kPa

2.2 Working fluids

Thanks to the wide range of organic fluids, ORCs can be designed for different heat source temperatures. On the other hand, having a wide range of fluid options to choose from complicates the optimization process [13]. In the present study, the list of potential working fluids was limited to hydrocarbons (HCs) and hydrofluorocarbons (HFCs). Both families of fluids have pros and cons. HCs are easily available at relatively low cost and are recognized as good working fluid candidates for heat recovery applications and geothermal power plants [13]. They are less harmful to the environment than other fluids (i.e., low GWP values and ODP=0). On the other hand, HCs are flammable, which can raise security concerns. As for HFCs, they are adequate for low-temperature heat sources [5, 22], but in general, they possess a relatively high GWP value (even though their ODP is close to 0). In this context, zeotropic binary mixtures of these fluids can be used in order to take advantage of the thermodynamic properties of both HCs and HFCs and, at the same time, limit the flammability and GWP of the working fluid. Based on the best options frequently reported in literature [15, 22–24], 6 HCs and 2 HFCs have been considered in the present work and are presented in Table 2. These fluids constitute the components of the binary mixtures that will be studied. All possible binary combinations of these fluids were analyzed, which constituted 28 possible mixtures. Mixing a wet and a dry fluid together can yield either a dry or a wet mixture, depending on the proportions of each component in the mixture. There are 12 of such mixtures among the 28 possible mentioned above. To facilitate the numerical implementation of the optimization procedure (described below in Section 3), each of these 12 mixtures was actually treated in the optimization process as two separate mixtures, i.e. one dry and one wet, each with its range of possible

compositions. Therefore, in the end, a series of 40 mixtures was simulated. Note that fluid properties were evaluated with REFPROP 9.1 [25].

Table 2. Working fluid components considered in this study.

Fluid	T_{Crit} [°C]	P_{Crit} [kPa]	Dry/Wet	Ref.
Pentane	196.6	3370	Dry	[15, 22, 24]
Isopentane	187.2	3380	Dry	[22, 23]
Neopentane	160.6	3196	Dry	[22]
R245fa	154	3650	Dry	[15, 22, 24]
Butane	152	3796	Dry	[15, 22– 24]
Isobutane	134.7	3630	Dry	[22, 24]
R134a	119	4640	Wet	[22, 24]
Propane	96.7	4250	Wet	[15, 22, 24]

2.3 ORC model

An ORC model was developed in Matlab®. The cycle is shown in Fig. 1 with its T-s diagram. Only subcritical cycles were evaluated in the present work and with both dry and wet mixtures. Four basic elements constitute the ORC. In the evaporator, the working fluid passes from state 1 to state 2 by recovering heat from the hot stream. The hot stream enters the evaporator at a temperature $T_{hs,in}$, which is assumed to be known. The working fluid enters the evaporator at a pressure lower than its critical pressure since only subcritical cycles were analyzed. Next, the working fluid expands through the turbine to produce power from state 2 to 3. The condenser cools down the working fluid to state 4 (saturated liquid at the low pressure P_L). A cold stream is used in order to do that, with an inlet temperature $T_{cs,in}$ at the condenser. Finally, a pump increases the pressure and brings back the working fluid to state 1. The following paragraphs explain under which assumptions each possible case was modeled.

It was supposed that the maximum allowable turbine inlet pressure was 90% of the mixture critical pressure. For dry mixtures, the turbine inlet temperature was the dew temperature for the corresponding evaporation pressure. However, wet mixtures were superheated until they reached a temperature 10°C below that of the heat source. The previous constraints were used to avoid numerical difficulties in the evaluation of thermophysical properties around the critical point, which can become quite problematic

for mixtures, since property database programs cannot provide accurate estimates of properties in the vicinity of the critical point [26, 27]. Superheating in the subcritical cycles was not considered for dry fluids because it is known in that case to only increase the system efficiency marginally, whereas the heat load to the condenser can increase due to the superheating that this type of fluid exhibits during expansion in the turbine [24]. Finally, the temperature difference of 10°C in the other conditions is used to ensure a proper heat transfer between the heat source and mixture working fluids.

Every process in the cycle is considered to be adiabatic and steady-state. Pressure drops were also neglected. Finally, a temperature rise of 7°C was fixed in the simulation for the cold fluid (sink) in order to avoid too high a temperature that could produce damage or thermal pollution.

The main equations employed in the thermodynamic model are presented below. The power invested in the pump is

$$\dot{W}_{pump} = \dot{m}_{mix}(h_1 - h_4), \tag{1}$$

with the enthalpy at state "1" given as

$$h_1 = h_4 + \left(\frac{h_{1,is} - h_4}{h_P}\right), \tag{2}$$

where $h_{1,is}$ is isentropic enthalpy at the pump outlet.

The turbine delivered power is

$$\dot{W}_T = \dot{m}_{mix}(h_2 - h_3), \tag{3}$$

with

$$h_3 = h_2 - h_T(h_2 - h_{3,is}), \tag{4}$$

where $h_{3,is}$ is the isentropic enthalpy at the turbine's outlet.

The heat added to the working fluid at the evaporator is

$$\dot{Q}_{Eva} = \dot{m}_{mix}\left(h_2 - h_1\right) = \dot{m}_{hs}\left(h_{hs,in} - h_{hs,out}\right). \tag{5}$$

The heat disposed at the condenser is

$$\dot{Q}_{Co} = \dot{m}_{mix}\left(h_3 - h_4\right) = \dot{m}_{cs}\left(h_{cs,out} - h_{cs,in}\right). \tag{6}$$

It is important to note that the heat exchangers and turbine were actually discretized as explained in Section 2.4.

The exergy destructed at the evaporator, turbine, condenser, and pump, respectively, are

$$\dot{I}_{Eva} = T_0 \dot{m}_{mix} \left[\left(s_2 - s_1 \right) + \left(s_{hs,in} - s_{hs,out} \right) \right], \quad (7)$$

$$\dot{I}_{T} = T_0 \dot{m}_{mix} \left(s_2 - s_3 \right), \quad (8)$$

$$\dot{I}_{Co} = T_0 \dot{m}_{mix} \left[\left(s_4 - s_3 \right) + \left(s_{cs,out} - s_{cs,in} \right) \right], \quad (9)$$

$$\dot{I}_{P} = T_0 \dot{m}_{mix} \left(s_1 - s_4 \right). \quad (10)$$

with T_0, which is 25 °C, being referred to as dead-state temperature.

The total exergy destructed within the cycle can be defined as

$$\dot{I}_{Total} = \dot{I}_{Eva} + \dot{I}_{T} + \dot{I}_{Co} + \dot{I}_{P} \quad (11)$$

Finally, the sink and heat source exergy flow (i.e., $\dot{E}_{cs}$ and $\dot{E}_{hs}$) are

$$\dot{E}_{cs} = \dot{m}_{cs} \left[\left(h_{cs,out} - h_{cs,in} \right) - T_0 \left(s_{cs,out} - s_{cs,in} \right) \right] \quad (12)$$

$$\dot{E}_{hs} = \dot{m}_{hs} \left[\left(h_{hs,in} - h_{hs,out} \right) - T_0 \left(s_{hs,in} - s_{hs,out} \right) \right] \quad (13)$$

Table 3 shows values used in the ORC modeling. It is important to emphasize that power cycles are notoriously influenced by the temperature limits between which they operate, i.e. heat source and cold sink temperatures. A single cold sink temperature representative of the ambient was used in the simulations, but as mentioned above different heat source temperatures were used in the optimization. The temperature of all other thermodynamic states of the power cycles are optimized as will be described below.

Table 3. Parameters and values assumed for the ORC modeling.

Parameter description	Value
Cold source (water)	
T_{cs}	25°C
P_{cs}	1000 kPa
Pump	
η_P	0.8
η_M	0.97
Turbine	
η_T	0.8
η_M	0.97

η_G	0.98
x_{min}	0.90
Dead state (air)	
Pressure	100 kPa
Temperature	22°C
Composition (mass fraction)	76% N_2, 23% O_2, 1% Ar.

2.4 Heat exchanger and turbine model

In the modeling of the two heat exchangers involved in the ORC, it was necessary to impose constraints in order to ensure that no violation of the second law occurred at any point within them. Essentially, this is achieved by ensuring that there is a minimal temperature difference (ΔT_{min}) between the hot and cold fluids everywhere in the heat exchanger.

Each heat exchanger was discretized into n elements and a heat balance was performed in each element. The enthalpy at the input (or output) of each element in each stream is calculated from:

$$h_{i+1,mix} = h_{i,mix} - \frac{\dot{Q}}{\dot{m}_{mix} n}; \; h_{i+1,hs} = h_{i,hs} - \frac{\dot{Q}}{\dot{m}_{hs} n}, \tag{14}$$

Subsequently the temperature of each stream of each i^{th}-element is easily determined by knowing its pressure and enthalpy, i.e.

$$T_{i+1,mix} = T\left(P_{mix}; h_{i+1,mix}\right); \; T_{i+1,hs} = T(P_{hs}; h_{i+1,mix}), \tag{15}$$

Finally, the temperature difference in all segment "i" is $\Delta T_i = T_{i,hs} - T_{i,mix}$, and it is verified that the minimal temperature difference is higher than the specified limit. If a design does not respect this constraint, it is eliminated.

When the ORC uses wet mixtures in a subcritical cycle, the blend can intersect the saturation curve and, consequently, liquid droplets could appear during the expansion in the turbine which could cause erosion. This problem can usually be avoided with a minimum quality (x_{min}) above 0.9 in the turbine [28]. In order to determine x_{min} it was necessary to divide the pressure drop between points 2 and 3 in Fig. 1 into small ΔP_i and verify that the minimal quality among the path from 2 to 3 was higher than the value indicated in Table 3. When the minimum quality was not respected, the cycle was simply discarded.

2.5 Model verification

Li et al. [29] also studied the impact of zeotropic mixtures on the performance of ORCs. No multiobjective optimization was attempted in that reference and several differences can be noted with the present work in terms of models and objectives (e.g., Li et al.'s work considers only one heat source temperature, did not consider the global conductance and exergy efficiency, fixed condensation conditions, etc.). Nevertheless, it is possible to use their results in some specific conditions to validate the present model and its numerical implementation. In order to do that, the energy equations were solved with the same conditions as is Ref. [29], using as working fluid a mixture of isobutane and R245fa with mass fractions of 0.3 and 0.7 respectively. The comparison between the results obtained with the present model and those from Ref. [29] are presented in Fig. 2. One can observe that the differences in thermal efficiency and power between the present model and that of the reference are small, with maximal variations of 1.3% and 2% respectively. The present model could thus be considered adequate. The small differences can be attributed to the fact that REFPROP 9 was used Ref. [29] whereas the 9.1 version is used here, as well as to the tolerance criteria used to declare convergence in the iterative calculations.

3. Multiobjective optimization problem

3.1 Objective functions and design variables

An optimization is defined by objective functions, design variables and constraints. This section formulates the optimization problem addressed in the present paper. When optimizing ORCs, several objectives are of interest. In the present work, the net power ($\dot{W}_{Net}$), exergy efficiency (η_{Exe}) and global conductance ($(UA)_{Total}$) were the three objective functions that were chosen. Note that the first two objectives are to be maximized, whereas the third is to be minimized. These objectives can be expressed using the following relations:

(i) Net power output ($\dot{W}_{Net}$): The net power is obtained by subtracting the power required by the pump from the power produced by the turbine:

$$\dot{W}_{Net} = \dot{W}_T \eta_M \eta_G - \frac{\dot{W}_P}{\eta_M} \tag{16}$$

where η_M and η_G are the mechanical and generator efficiencies (see Table 3).

(ii) Second-law efficiency (η_{Exe}): The exergy efficiency is defined as the ratio of the useful exergy obtained to the exergy consumed by system [30] :

$$\eta_{Exe} = 1 - \frac{\dot{I}_{Total} + \dot{E}_{Co}}{\dot{E}_{hs}} \tag{17}$$

(iii) Size of heat exchangers (i.e., $(UA)_{Total}$ value): the size of the system can be assessed by the total heat exchanger conductance:

$$(UA)_{Total} = (UA)_{Eva} + (UA)_{Co} \tag{18}$$

The UA values were evaluated with the logarithmic mean temperature difference method (LMTD), remembering that a discretization of each heat exchanger is needed in order to consider the variation of the working fluid properties as recommended in Ref. [31]. Considering a counterflow heat exchanger, a heat balance on one sub-section yields:

$$(UA)_i = \frac{\dot{Q}_i}{\left[\left(T_{H,i+1} - T_{C,i}\right) - \left(T_{H,i} - T_{C,i+1}\right)\right]} \left[\ln\left\{ \frac{\left(T_{H,i+1} - T_{C,i}\right)}{\left(T_{H,i} - T_{C,i+1}\right)} \right\} \right]^{-1} \tag{19}$$

By summing Eq. (19) over all segments, one obtains the total UA value for this heat exchanger.

The goal of the optimization process is to identify the best values for the design variables. This is achieved by allowing the design variables to vary within predefined bounds. In the present optimization process, the design variables and their bounds were:

- Pressure at the evaporator (P_2): the minimal value was 100 kPa and, as mentioned previously, the maximal value was chosen to be 90% of the critical pressure:

  $$P_2 \in [100\ \text{kPa}, 0.9 P_{Crit}]$$

  Note that the inferior limit was adjusted to avoid negative pressures, which would increase the complexity and cost of the system [13, 24].

- Condensation temperature of the mixture (T_{Co}): the lower bound was 28°C and the upper bound was 10°C below the bubble temperature at the pressure P_2, i.e.:

  $$T_{Co} \in \left[28\ °\text{C}, T_{bubble\ @\ P_2} - 10\ °\text{C}\right]$$

  Note that the lower bound corresponds to the cooling fluid temperature T_{cs} plus 3°C.

- Minimal temperature difference in the evaporator (ΔT_{min}): this value was allowed to vary between 4 and 15°C:

$$\Delta T_{min} \in [4\ °C, 15\ °C]$$

  From the ΔT_{min} value and the thermodynamic state points of the cycle, the mixture mass flow rate was calculated.

- As mentioned previously, the wet mixtures can be superheated before entering the turbine. Therefore, the temperature of the mixture at the inlet of the turbine ($T_{2,wet}$) has been chosen as another design variable to optimize in cycles with wet mixtures. Its lower value was the dew point of the mixture at the pressure P_2, and its upper value was the heat source fluid temperature minus 10°C, i.e.:

$$T_{2,wet} \in \left[T_{dew@P_2}, T_{hs,in} - 10\ °C \right]$$

The fluid mixture was also considered as a design variable. It was optimized sequentially. First, two fluids were specified to form the mixture. The proportion of each constituent in the mixture was represented by the variable ϕ, i.e. the proportion of the first fluid in the mixture, which could range from 0.01 (~pure fluid 1) to 0.99 (~pure fluid 2). This variable ϕ was optimized along with the other variables listed above. The choice of the two components to form the mixture was not considered as a design variable per se, but the optimization approach was applied systematically to the list of 28 possible mixtures described above. Therefore, after all simulations, it was possible to determine which mixture was optimal in each case by comparing the results obtained for each binary combination of pure fluids.

3.2 Optimization procedure

As can be seen from the previous sections, it is impossible to identify manually the best set of design variables in terms of the three objective functions mentioned above. In order to optimize simultaneously these different objectives, a multi-objective genetic algorithm (GA) was used. Genetic algorithms are a class of evolutionary algorithms based on the principles of genetics and natural selection, which have been used to identify global optima, even for discontinuous, non-differentiable and highly non-linear functions. In GAs, different values of the design variables are generated randomly to form an initial population. Based on their fitness (i.e., best designs are more likely to reproduce) and on

operations such as crossovers and mutations, a new generation of designs is generated. The best designs from a generation are also allowed to propagate directly to the next generation. This procedure is repeated over a certain number of generations. For multi-objective optimization problems, as the search is performed over successive generations, the population evolves toward a set of solutions called a Pareto front or non-dominated set [32]. Each point on this front is considered "optimal" in the sense that it is not possible to improve one of the objective functions for this point without degrading one or more of the other objective functions. Posteriorly, designers could select which design point to choose on the front for a project depending on the importance given to each of the objectives. The multi-objective GA optimization algorithm was NSGA-II, a recognized approach for which optimization flowcharts and other details can easily be found in literature [32] [33] [34]. The reasons why NSGA-II was chosen among other techniques are its capacity to handle non-linearity, discrete and continuous design variables, multiple objective functions, and its relative easiness to use.

The parameters of the GA used in this work are: the size of the population is 600, the number of generations that was performed for each optimization is 60, the crossover fraction is 0.7 and the number of elites propagating from one generation to the next is 10. The other parameters were left to the default value of the toolbox that was used [33]. Note that the population size is relatively large in order to obtain well-defined Pareto fronts with a sufficient number of points. Furthermore, different tests were performed by varying the number of generations, and it was found that changes to the Pareto fronts were negligible when the number of generation was increased further, but that the computational cost increased significantly.

4. Results and discussions

4.1 Multi-fluid optimized Pareto fronts

The optimization procedure described above was first applied to the scenarios in which the heat source temperature was equal to 180°C. Fig. 3 shows the resulting Pareto fronts (i.e. non-dominated solutions in terms of η_{Exe}, $\dot{W}_{Net}$ and $(UA)_{Total}$) for both dry and wet mixtures in 3D. Note that the optimization results for all 28 mixtures, with any compositional fraction, are shown in this figure. In other words, each point in Fig. 3 is the result the

optimization procedure introduced in Section 3 for a given binary mixture. An important aspect of Fig. 3 is the shape or three-dimensionality portrayed by the numerous optimization points reported, which supports the use of multi-objective optimization techniques. For instance, optimized scenarios for dry mixtures with the lowest $(UA)_{Total}$-values can present a relatively high η_{Exe}-values and low $\dot{W}_{Net}$-values, or vice-versa (i.e. low η_{Exe}-values and high $\dot{W}_{Net}$).

The competition between each two objective functions becomes clearer in Fig. 4, which shows projections of the Pareto fronts in order to facilitate the analysis two objective functions at the time. In Fig. 4a, which shows $\dot{W}_{Net}$ vs $(UA)_{Total}$, it appears clearly that for a given size of the heat exchangers (i.e. $(UA)_{Total}$ value), the dry mixtures produce more net power output $\dot{W}_{Net}$ compared to wet mixtures. Furthermore, increasing $\dot{W}_{Net}$ above 50 kW and 60 kW for wet and dry mixtures respectively, leads to a sharp increase of the required $(UA)_{Total}$. Fig. 4b depicts the impact of η_{Exe} on $(UA)_{Total}$. As presented above, it can be verified that increments in η_{Exe} is accompanied by an augmentation of the conductance of the heat exchangers, both for wet and dry mixtures. On the other hand, it can be verified in Fig. 4c that many non-dominated solutions for dry mixtures provide very low values of $\dot{W}_{Net}$, and depending on their compositions, these mixtures can exhibit various values of η_{Exe}. This comes from the fact that in these conditions, the heat source fluid experiences only a small reduction of temperature as it passes in the evaporator, which yields a cycle producing less power, and requiring a smaller value of $(UA)_{Total}$.

The results presented in Figs. 3 and 4 for the evaluated mixtures allow identifying general trends for the optimal solutions of each work fluid regarding the three objective functions. However, the best mixtures for this temperature level (180°C) cannot be identified from these figures. In order to do that, a second step in the optimization procedure is required, and consists in applying a non-dominated sorting (NDS) method [34] considering all the Pareto fronts achieved for each individual mixture. This allows generating a single Pareto front of non-dominated solutions that consider the optimization of the choice of mixture. After the application of the NDS algorithm, 884 optimal solutions for this temperature level (i.e., heat source temperature of 180°C) were found and are reported in Fig. 5a on a plane $\dot{W}_{Net}$ - $(UA)_{Total}$ (see rightmost curve). Among these 884 points, 22 types of mixtures, with varied compositional fractions, were identified. These

mixtures were all dry, i.e. formed from two dry fluids or by mixing a dry and a wet fluid with a low fraction of the wet fluid in the mixture.

In a similar way, the NDS algorithm was applied to the set of optimal solutions achieved for each heat source temperature level described in Section 2.1 in order to obtain global Pareto fronts, as shown by the other five curves presented in Fig. 5a. As expected, other optimal solutions were found on the Pareto fronts as the heat source temperature was decreased (i.e. 1312, 1393, 4111, 1422 and 1304 solutions for temperature levels of 80°C, 100°C, 120°C, 140°C and 160°C respectively). This shows that many solutions in terms of working fluid mixtures are available in each segment of the Pareto fronts. The dry mixtures continue to be the best working fluids, i.e. the ones constituting the dominant solutions, for a heat source temperature of 160°C. On the other hand, the wet mixtures (composed mostly of R134a, propane or their combination) prove to be part of the optimal solutions for heat source temperature of 140°C and below. Furthermore, one should also note that the color represents the exergy efficiency for each optimal point that constitutes the front. In general, one can see reductions of $\dot{W}_{Net}$ and $(UA)_{Total}$ for cooler heat sources.

For the sake of comparison, the optimization procedure was repeated, this time with pure fluids only. A heat source at 180°C was assumed for that case. In Fig. 5b, the resulting Pareto fronts for pure fluids are compared to the Pareto front achieved with mixtures that was previously shown in Fig. 5a. It can be seen that allowing the optimization of the fluid mixture composition yield better solutions, since it provides more degrees of freedom to optimize the cycle.

4.2 Working fluid optimization

Because of the large number of optimal solutions for each temperature level, it becomes a challenge to establish how different mixtures are distributed along each Pareto front shown in Fig. 5. In order to develop a better understanding of which mixtures are best, Figs. 6a to 6b present the pure fluid percentages that compose the mixtures in each $\dot{W}_{Net}$-level achievable for the heat source temperatures of 180°C and 80°C, respectively, and the percentage of mixtures which contained these pure fluids. For instance, for a heat source of 180°C, Fig. 6a indicates that pentane is the pure fluid that is the more widely used for the composition of mixtures up to 40 kW, whereas R245fa is the preferred pure fluid in

mixtures for high power cycles (>50 kW). The highest values of power, and consequently of η_{Exe} and $(UA)_{Total,}$ are reached with mixtures made of R245fa, pentane, isopentane and neopentane. Fig. 6b establishes that up to ~4 kW, isopentane and pentane form approximately 40% of the mixtures that are found among the optimal solutions when the heat source temperature is 80°C. Above that net power value, the mixtures are mostly composed with isopentane and R245fa. For the 80°C temperature level, when R134a and propane are mixed with the other fluids, they can form mixtures that can be either dry or wet depending on the proportion of each fluid in the mixture. Therefore, these two fluids do not constitute any of the mixtures with which the high power values were achieved. Finally, two general observations can be made from Fig. 6. First, one notes again the large number of possible designs and mixtures to reach a certain value of $\dot{W}_{Net}$ (or of the other objectives). Second, almost all mixtures that were evaluated can bring adequate solutions, especially in intermediate regions of the Pareto fronts. This is especially true for relatively low temperature values of the heat source (e.g., 80°C), since the difference in $\dot{W}_{Net}$ is small in absolute terms, and the composition of optimal mixtures becomes less influential.

For each point on the Pareto front, the optimal mass fraction was noted and the occurrence of optimal mass fraction for the two temperature limits analyzed previously are presented in Figs. 7a (180°C) and 7b (80°C). Again, for a mixture A/B, a fraction of 0 means that only A is present in the mixture, and a fraction of 1 means that only B is present. It can be observed that when the heat source temperature was 180°C, more than 50% of the optimal mixtures on the Pareto front were constituted with a mass fraction of ~1, i.e. the proportion of one of the two pure fluids forming the binary mixture is small. In other words, 50% of the optimal designs were essentially obtained using a nearly pure fluid. In that case, pentane is actually the dominant component of these mixtures as it is possible to find mixtures rich in pentane (i.e. with fraction close to 1) in almost all positions of the curve of Fig. 5, except for large values of $\dot{W}_{Net.}$ In the case with a heat source temperature of 80°C, the optimal mass fraction is more evenly spread, and most compositions have an optimal fraction between 0.2 and 0.7. Approximately 25% of the optimal mixtures have one of their two components with a mass fraction superior to 0.9. Pentane, isopentane and R245fa correspond to the pure fluids that appear more frequently in the mixtures with this characteristic. Finally, it should be noted that in both temperature levels, the mixtures in

which one of the two components has a mass fraction of ~1 are not found in regions of the Pareto fronts with large values of $\dot{W}_{Net}$.

In accordance with the results presented above, it is visible that there is a large number of available mixtures in order to achieve the best values of $\dot{W}_{Net}$, η_{Exe} and $(UA)_{Total}$ in all segments of the Pareto front and for each heat source temperature level. Consequently, identifying a unique "best" work fluid mixture is impossible, particularly given that three objectives were considered. The choice of a cycle configuration, including the choice of the work fluid mixture, depends on the weight put on each objective in the decision-making process.

4.3 Behavior of dependent variables on Pareto fronts

Regarding the optimal operational variables, Fig. 8 presents the values of $\dot{m}_{cs}$, T_{Co} and P_{Eva} through the right hand side color scale for the optimal solutions on the Pareto front for the heat source at 180°C. It is clear from Fig. 8a that the progressive augmentation of the three objectives along the front is accompanied by an augmentation of the flow rate of the cooling fluid, $\dot{m}_{cs}$. In practice, in order to limit the energy consumption of the auxiliary equipment of the cooling system (not taken into account in the present work), the value of $\dot{m}_{cs}$ should be kept within 7-11 kg/s, which could guide cycle designers in selecting certain combinations over others in the Pareto front. The optimal condensation temperature, which is shown in Fig. 8b, demonstrates two clear trends. First, one notes the significant raise of the condensing temperatures to very high values as $\dot{W}_{Net} \rightarrow 0$ and $(UA)_{Total} \rightarrow 0$. Second, the mixtures that exhibit sounder values of the objective functions have a condensing temperature in the range between 38 and 49°C, which is relatively higher than the lower limit that was fixed for this parameter, i.e. 28°C. The evaporation pressure in Fig. 8c does not exhibit a continuous evolution along the front as the other variables. This comes from the fact that mixtures change in the front and that different evaporation pressure are required depending on the fluid. Although relatively low pressures are found (as low as ~1000 kPa), in order to achieve high net power values, it is required to increase P_{Eva}. It was also observed that the optimal evaporator pressure was always between 0.3 and 0.9 the critical pressure of the mixture.

4.4 $(UA)_{Total}$ normalization of the optimized Pareto solutions

In order to further identify the best mixture options, Fig. 9 reports the net power output per unit of heat exchanger conductance, i.e. $\dot{W}_{Net}/(UA)_{Total}$, versus the exergy efficiency. $\dot{W}_{Net}/(UA)_{Total}$ is an interesting figure of merit, which indicates the cycle's productivity, and a value as high as possible is desirable. It is visible that some designs maximize this criterion, which comes from the fact that, as seen previously, in order to reach the largest values of $\dot{W}_{Net}$, the heat exchangers size would become prohibitively large, which will reduce $\dot{W}_{Net}/(UA)_{Total}$ on the right hand side of Fig. 9. On the other hand, in the left part of Fig. 9, the net power is close to zero, which means that $\dot{W}_{Net}/(UA)_{Total}$ becomes very small for modest exergy efficiency values. Table 4 presents the solutions having variations of less than 1% of the maximal possible value of $\dot{W}_{Net}/(UA)_{Total}$ for each temperature level. It can be verified that the working fluids for which this figure of merit is maximal are mostly made of pentane and isopentane for each temperature levels, even though the operational parameters can vary strongly for each optimal design.

Table 4. Optimal mixtures and maximal $\dot{W}_{Net}/(UA)_{Total}$ for each heat source temperature considered.

Temp. [°C]	Mixture	$\dot{W}_{Net}/(UA)_{Total}$ [K]	Dry/Wet	ϕ^*	T_{Co} [°C]	P_{Eva} [kPa]	$\dot{m}_{cs}$ [kg/s]
180	Pentane/Isopentane	1.89	Dry	0.33	65.45	2149.49	1.55
	Pentane/Isopentane	1.88	Dry	0.47	59.26	2013.01	2.59
	Pentane/Propane	1.88	Dry	0.99	53.91	2087.38	0.92
	Pentane/R245fa	1.88	Dry	0.99	58.32	1788.52	3.25
	Pentane/Isopentane	1.88	Dry	0.59	57.84	1968.45	2.63
	Pentane/Isopentane	1.87	Dry	0.43	59.60	2135.15	1.76
	Pentane/R245fa	1.87	Dry	0.98	58.75	1888.28	2.57
160	Isopentante/Isobutane	1.58	Dry	0.99	58.44	1677.83	0.82
	Isopentante/Neopentane	1.57	Dry	0.90	55.77	1661.94	1.71
	Pentane/Isopentane	1.57	Dry	0.40	56.71	1543.76	1.00
	Isopentante/Neopentane	1.56	Dry	0.80	56.50	1893.54	0.47
	R245fa/Butane	1.56	Dry	0.04	56.20	3414.55	0.46
140	Pentane/Isopentane	1.24	Dry	0.60	49.35	983.53	1.32
	Pentane/Isopentane	1.24	Dry	0.59	49.66	989.75	1.26
	Pentane/Isopentane	1.23	Dry	0.58	49.55	1074.48	0.45
120	Pentane/Isopentane	0.93	Dry	0.59	51.13	721.51	0.23
	Pentane/Isopentane	0.92	Dry	0.27	47.66	705.30	0.98
100	Pentane/Isopentane	0.62	Dry	0.61	46.50	446.72	0.42
	Pentane/Isopentane	0.62	Dry	0.64	45.01	435.88	0.56
80	Pentane/Isopentane	0.35	Dry	0.56	40.58	280.75	0.19
	Isopentane/Propane	0.35	Dry	0.99	37.60	361.68	0.002

Pentane/Isopentane	0.35	Dry	0.52	40.18	290.26	0.14

*ϕ represents the fraction of A within an A/B mixture.

5. Scale analysis

In order to develop a better understanding of which mixtures and operational parameters are best, a scale analysis is proposed in this section. A heat balance in the evaporator reveals that $\dot{Q} \sim (UA)_{Eva} \Delta T_H \sim \dot{m}_{wf} h_{fg}$, i.e.:

$$(UA)_{Eva} \sim \frac{\dot{m}_{wf} h_{fg}}{\Delta T_H} \tag{20}$$

where ΔT_H is the characteristic temperature difference between the heat source fluid and the working fluid. With a similar balance in the condenser, one can express the total heat exchanger conductance as:

$$(UA)_{Total} \sim \frac{2\dot{m}_{wf} h_{fg}}{\Delta T}, \tag{21}$$

where, in order to simplify the analysis, it was assumed that $\Delta T_H \sim \Delta T_C$, and the characteristic temperature difference was labelled simply ΔT.

The power output can be written at $\dot{W} \sim \dot{m}_{wf}(h_2 - h_3)$, where states 2 and 3 are shown in Fig. 1 (inlet and outlet of turbine, respectively). Then, applying an analysis as proposed in Ref. [5], it can be shown that:

$$\dot{W} \sim \dot{m}_{wf} c_{wf} \left[(T_H - T_C) - 2\Delta T - \frac{\dot{m}_{wf} h_{fg}}{\dot{m}_H c_H} \right], \tag{22}$$

where T_H and T_C are the temperatures of the heat source and of the sink. $\dot{W}$ can be maximized with respect to the working fluid flow rate. Deriving Eq. (23) with respect to $\dot{m}_{wf}$, and equaling to zero, one finds:

$$\begin{aligned} \frac{\dot{m}_{wf,opt}}{\dot{m}_H} &= \frac{\Delta T_{global} - 2\Delta T}{2h_{fg}/c_H} \\ \frac{\dot{W}_{max}}{\dot{m}_H} &= \frac{[(T_H - T_C) - 2\Delta T]^2}{4h_{fg}/(c_H c_{wf})} \end{aligned}. \tag{23}$$

where again $\dot{m}_H$ is equal to 1 kg/s. Combining Eqs. (21) and (23), one finds and expression for ΔT:

$$\Delta T \sim \frac{T_H - T_C}{\frac{(UA)_{Total}}{\dot{m}_H c_H} + 2}, \tag{24}$$

which can be introduced back in the expression of the maximal net work in Eq. (23):

$$\frac{\dot{W}_{max}}{\dot{m}_H} \sim \frac{(T_H - T_C)^2}{4h_{fg}/(c_H c_{wf})} \left(\frac{NTU}{2 + NTU} \right)^2, \tag{25}$$

where NTU is $(UA)_{Total}/(\dot{m}_H c_H)$. Eq. (25) shows the expected relation between two of the objective functions (i.e., $\dot{W}_{max}$ vs. UA) in the optimized designs, as a function of the overall temperature difference ($T_H - T_C$).

To determine whether the scaling analysis described above matches the Pareto front and NDS results reported thus far, Fig. 10 shows the numerically optimized data presented in Fig. 5, which is now reported in terms of $\dot{W}_{max}$ as a function of $[NTU/(2+NTU)]^2$, for the different temperature levels investigated here – see open symbols. Next, by comparing the numerically optimized data with the scaling $\dot{W}_{max}$ results obtainable from Eq. (25), one can observed that both solutions agree within less than ±10 % if the scaling results are multiplied by single fitting constant 2.898×10^{-3} kJ/kg.K^2 regardless of its heat source temperature. Note that the fitting started for $[NTU/(2+NTU)]^2 \geq 0.1$ and that the agreement above encompasses approximately 83% of the numerical optimized data points. The scaling results are shown in Fig. 10 through the solid straight lines, which can be readily obtained through a constant-adjusted version of Eq. (25), which reads

$$\frac{\dot{W}_{max}}{\dot{m}_H} = 0.002898(T_H - T_C)^2 \left(\frac{NTU}{2 + NTU} \right)^2. \tag{26}$$

The importance of the above analysis is that any designer considering the use of one of the binary mixtures tested in the present study as working fluid in an ORC, while

knowing T_H, T_C and NTU, is capable of analytically determining $\dot{W}_{max}$ with good precision through Eq. (26), which can be used as a reference.

As for the optimal selection of mixtures, based on the above analysis, the following can be said:

(i) In order to have a working fluid that is not supercritical in the evaporator, one needs: $T_H - \Delta T < T_{Crit}$. Given Eq. (24), this means:

$$\frac{NTU+1}{NTU+2} \lesssim \frac{T_{Crit} - T_C}{T_H - T_C} \tag{27}$$

This inequality was respected for the optimal designs introduced above, except when the heat source temperature and NTU value were high. This is because, in writing Eq. (27), the order of magnitude of the approach temperature ΔT is obtained with Eq. (24). However, for large NTU values, ΔT in Eq. (24) can tend to zero, which is in contradiction with the minimal temperature differences imposed in the model (See Section 2), and a more realistic expression for ΔT at large NTU value such as $\Delta T \sim$ MAX(Eq. (24); ΔT_{min}) would be required. During the course of the optimization process, the optimized mixtures should exhibit a critical temperature that is high enough to keep the cycle subcritical, in particular with a high source temperature. When the temperature difference between the heat source and the working fluid becomes small ($\Delta T \rightarrow 0$), one finds NTU $\rightarrow \infty$. The left hand side of Eq. (27) becomes 1, in which case the critical temperature of the mixture should be above ~180°C (i.e., when NTU is large and the source temperature is at 180°C). This could limit the recourse to R134a and propane in the optimal mixtures since their critical temperature is lower than these limits (see Table 1).

(ii) Optimal mixtures present low h_{fg}/c_{wf} ratios, see Eq. (25). Although the latent heat of a mixture and its specific heat depends on pressure, temperature and composition, the fitting of Eq. (13) reveals that in the optimized designs obtained in this work, one actually finds: $h_{fg}/(c_{wf}c_H) \sim 360.6$ K (using 4.18 kJ/kg.K for c_H). To illustrate this statement, the ratio h_{fg}/c_{wf} was calculated in the evaporator of the optimized designs. It was found that the average value of this ratio was 358.37 K with a standard deviation of

132.53 K, which corroborates this analysis, in a scaling sense. The criterion on h_{fg} / c_{wf} could be used in the design process of the working fluid mixture.

6. Conclusions

The use of binary mixtures in ORC can have numerous advantages as previously discussed. However, so far, there is no consensus as to which are the best mixtures for a certain heat source temperature. Therefore, the present analysis considers up to twenty-eight different binary mixtures that are possible working fluid candidates for a basic ORC. The search for the ideal mixtures is performed by allowing the ORC to experience several heat source temperature values while using a genetic algorithm optimization routine to identify which mixtures return the highest values of net power and exergetic efficiency and the lowest values of global conductance. The selection of the best solutions obtained with the optimization routine is done by combining the Pareto front and non-dominant sorting methods.

The results show that, generally speaking, high values of net power are associated with high values of exergetic efficiency and global conductance – note that, ideally, low values of global conductance are desirable. More importantly, however, is that, while it is not possible to identify a single mixture that returns the best values of the objective functions considered, for high heat source temperatures (i.e., 180 °C), fluids such as R245fa and propane are the dominant fluids within the best mixtures (~ 50 %). Differently, as the heat source temperature is reduced (i.e., 80 °C), a wide range of mixtures perform alike.

Also, a scaling analysis aiming to determine the maximal specific net power produced ($\dot{W}_{max}$) by the ORC as a function of the high and low-end temperatures, and the Number of Transfer Units (NTU) is proposed. The scaling solution is directly compared with the sorted results obtained from the genetic algorithm, only differing by a single constant value for all heat source temperature levels considered. Therefore, the scaling solution for $\dot{W}_{max}$ was corrected with the adjusting constant and can be used a reference parameters for designer interested in ORC.

Finally, other objective functions, such as life-cycle GWP working fluid [35], could be included in future work. In fact, as reducing the environmental impact of working fluids

in power and refrigeration cycles continues to be a necessity, the importance of the environmental footprint of working fluids is constantly increasing. Furthermore, future work could include cost (purchase and operational) as an objective function to be minimized, which would require appropriate correlations or data to estimate the cost of the main pieces of equipment of the cycle. Finally, multi-criteria analysis tools could be developed from the Pareto fronts presented here to help the decision-making in the design of an ORC and provide an adequate weight to each objective function in a given context.

Acknowledgements

The "Emerging Leaders in the Americas Program" (ELAP) of the Government of Canada supported the visit of the first author to Université Laval. The first and last authors also appreciate the support obtained from Petrobras/ANNEL (grant PD-0553-0023/2012). The second author's work was supported by the Natural Sciences and Engineering Research Council of Canada (NSERC) and the Institut de recherche d'Hydro-Québec (IREQ) via the grant RDCPJ 467685-14.

References

[1] D. Meinel, C. Wieland, and H. Spliethoff, "Economic comparison of ORC (Organic Rankine cycle) processes at different scales," *Energy*, vol. 74, pp. 694–706, Sep. 2014.

[2] S. Quoilin, "Sustainable energy conversion through the use of Organic Rankine Cycles for waste heat recovery and solar applications," University of Liège, Liège, Belgium, 2011.

[3] K. Rahbar, S. Mahmoud, R. K. Al-Dadah, N. Moazami, and S. A. Mirhadizadeh, "Review of organic Rankine cycle for small-scale applications," *Energy Convers. Manag.*, vol. 134, pp. 135–155, Feb. 2017.

[4] A. Habibzadeh and M. M. Rashidi, "Thermodynamic Analysis of Different Working Fluids Used in Organic Rankine Cycle for Recovering Waste Heat from Gt-Mhr," *J. Eng. Sci. Technol.*, vol. 11, no. 1, pp. 121–135, Jan. 2016.

[5] N. Chagnon-Lessard, F. Mathieu-Potvin, and L. Gosselin, "Geothermal power plants with maximized specific power output: Optimal working fluid and operating conditions of subcritical and transcritical Organic Rankine Cycles," *Geothermics*, vol. 64, pp. 111–124, Nov. 2016.

[6] J. Haervig, K. Sorensen, and T. J. Condra, "Guidelines for optimal selection of working fluid for an organic Rankine cycle in relation to waste heat recovery," *Energy*, vol. 96, pp. 592–602, Feb. 2016.

[7] J. L. Wang, L. Zhao, and X. D. Wang, "A comparative study of pure and zeotropic mixtures in low-temperature solar Rankine cycle," *Appl. Energy*, vol. 87, no. 11, pp. 3366–3373, Nov. 2010.

[8] H. Chen, D. Y. Goswami, M. M. Rahman, and E. K. Stefanakos, "A supercritical Rankine cycle using zeotropic mixture working fluids for the conversion of low-grade heat into power," *Energy*, vol. 36, no. 1, pp. 549–555, Jan. 2011.

[9] M. Chys, M. van den Broek, B. Vanslambrouck, and M. De Paepe, "Potential of zeotropic mixtures as working fluids in organic Rankine cycles," *Energy*, vol. 44, no. 1, pp. 623–632, Aug. 2012.

[10] F. Heberle, M. Preißinger, and D. Brüggemann, "Zeotropic mixtures as working fluids in Organic Rankine Cycles for low-enthalpy geothermal resources," *Renew. Energy*, vol. 37, no. 1, pp. 364–370, Jan. 2012.

[11] J. G. Andreasen, U. Larsen, T. Knudsen, L. Pierobon, and F. Haglind, "Selection and optimization of pure and mixed working fluids for low grade heat utilization using organic Rankine cycles," *Energy*, vol. 73, pp. 204–213, Aug. 2014.

[12] D. Luo, A. Mahmoud, and F. Cogswell, "Evaluation of Low-GWP fluids for power generation with Organic Rankine Cycle," *Energy*, vol. 85, pp. 481–488, Jun. 2015.

[13] Ennio Macchi, *Organic Rankine Cycle (ORC) Power Systems - ScienceDirect*. Elsevier Science, 2016.

[14] Y. Wu, Y. Zhu, and L. Yu, "Thermal and economic performance analysis of zeotropic mixtures for Organic Rankine Cycles," *Appl. Therm. Eng.*, vol. 96, pp. 57–63, Mar. 2016.

[15] K. Braimakis, M. Preißinger, D. Brüggemann, S. Karellas, and K. Panopoulos, "Low grade waste heat recovery with subcritical and supercritical Organic Rankine Cycle based on natural refrigerants and their binary mixtures," *Energy*, vol. 88, pp. 80–92, Aug. 2015.

[16] P. Collings, Z. Yu, and E. Wang, "A dynamic organic Rankine cycle using a zeotropic mixture as the working fluid with composition tuning to match changing ambient conditions," *Appl. Energy*, vol. 171, pp. 581–591, Jun. 2016.
[17] M. Sadeghi, A. Nemati, A. ghavimi, and M. Yari, "Thermodynamic analysis and multi-objective optimization of various ORC (organic Rankine cycle) configurations using zeotropic mixtures," *Energy*, vol. 109, pp. 791–802, Aug. 2016.
[18] Y. Feng, T. Hung, K. Greg, Y. Zhang, B. Li, and J. Yang, "Thermoeconomic comparison between pure and mixture working fluids of organic Rankine cycles (ORCs) for low temperature waste heat recovery," *Energy Convers. Manag.*, vol. 106, pp. 859–872, Dec. 2015.
[19] Oyeniyi A. Oyewunmi and Christos N. Markides, "Thermo-Economic and Heat Transfer Optimization of Working-Fluid Mixtures in a Low-Temperature Organic Rankine Cycle System," *Energies*, vol. 9, no. 6, p. 448, Jun. 2016.
[20] J. M. Cardemil and A. K. da Silva, "Parametrized overview of CO2 power cycles for different operation conditions and configurations – An absolute and relative performance analysis," *Appl. Therm. Eng.*, vol. 100, pp. 146–154, May 2016.
[21] F. G. Battisti, J. M. Cardemil, F. M. Miller, and A. K. da Silva, "Normalized performance optimization of supercritical, CO2-based power cycles," *Energy*, vol. 82, pp. 108–118, Mar. 2015.
[22] J. Bao and L. Zhao, "A review of working fluid and expander selections for organic Rankine cycle," *Renew. Sustain. Energy Rev.*, vol. 24, pp. 325–342, Aug. 2013.
[23] M. Pasetti, C. M. Invernizzi, and P. Iora, "Thermal stability of working fluids for organic Rankine cycles: An improved survey method and experimental results for cyclopentane, isopentane and n-butane," *Appl. Therm. Eng.*, vol. 73, no. 1, pp. 764–774, Dec. 2014.
[24] H. Chen, D. Y. Goswami, and E. K. Stefanakos, "A review of thermodynamic cycles and working fluids for the conversion of low-grade heat," *Renew. Sustain. Energy Rev.*, vol. 14, no. 9, pp. 3059–3067, Dec. 2010.
[25] NIST, "REFPROP Version 9.1. NIST 2013." Available in: https://www.nist.gov/srd/nist23.cfm.
[26] L. Pan, H. Wang, and W. Shi, "Performance analysis in near-critical conditions of organic Rankine cycle," *Energy*, vol. 37, no. 1, pp. 281–286, Jan. 2012.
[27] L. Pan, X. Wei, and W. Shi, "Performance analysis of a zeotropic mixture (R290/CO2) for trans-critical power cycle," *Chin. J. Chem. Eng.*, vol. 23, no. 3, pp. 572–577, Mar. 2015.
[28] Michael J. Moran, Howard N. Shapiro, Daisie D. Boettner, and Margaret B. Bailey, *Fundamentals of Engineering Thermodynamics*, 7th ed. Wiley, 2010.
[29] Y.-R. Li, M.-T. Du, C.-M. Wu, S.-Y. Wu, and C. Liu, "Potential of organic Rankine cycle using zeotropic mixtures as working fluids for waste heat recovery," *Energy*, vol. 77, pp. 509–519, Dec. 2014.
[30] Feidt Michel, *Thermodynamique et optimisation énergétique des systèmes et procédés*. Lavoisier Tec. & Doc., 1996.
[31] Gregory Nellis and Sanford Klein, *Heat Transfer*. Cambridge: Cambridge University Press, 2009.
[32] Kalyanmoy Deb, *Multi-Objective Optimization using Evolutionary Algorithms*. Willey, 2001.

[33] MathWorks,217,Available: https://www.mathworks.com/help/gads/gamultiobj.html.
[34] K. Deb, A. Pratap, S. Agarwal, and T. Meyarivan, “A fast and elitist multiobjective genetic algorithm: NSGA-II,” *IEEE Trans. Evol. Comput.*, vol. 6, no. 2, pp. 182–197, Apr. 2002.
[35] J. Frutiger, J. Andreasen, W. Liu, H. Spliethoff, F. Haglind, J. Abildskov, G. Sin, “Working fluid selection for organic Rankine cycles – Impact of uncertainty of fluid properties,” Energy, vol. 109, pp. 987–997, Aug. 2016.

Figure captions

Figure 1 a) Basic Rankine cycle configuration and b) T-s diagram of the subcritical ORC studied in this work (example with a mixture of Isopentane/R245fa with 0.63 Isopentane mass fraction), where BP and DP indicate the bubble and dew temperatures, respectively.

Figure 2 Numerical model validation with data published in Ref. [29] with a mixture of Isobutane/R245fa with Isobutane mass fraction of 0.7.

Figure 3 Pareto fronts for dry and wet mixtures with heat source temperature of 180°C.

Figure 4 Pareto fronts projections a) $\dot{W}_{Net}$ - $(UA)_{Total}$, plane, b) η_{Exe} - $(UA)_{Total}$, plane and c) $\dot{W}_{Net}$ - η_{Exe}, plane, with heat source of 180°C.

Figure 5 a) Pareto fronts for mixtures with heat source temperatures between 80°C and 180°C after applying the Non domination sorting method, and b) Pareto fronts obtained with a pure fluids with a heat source at 180°C.

Figure 6 Percent of blends for given fluid as a function of $\dot{W}_{Net}$ for: a) 180 °C and b) 80°C.

Figure 7 Percent of mass fraction occurrence for: a) 180°C and b) 80°C.

Figure 8 Optimal values of objective functions for 180°C heat source as a function of a) $\dot{m}_{ss}$, b) T_{Co} and c) P_{Eva}.

Figure 9 Normalization of $\dot{W}_{Net}/(UA)_{Total}$ for Non-Dominations-Solutions for temperature levels of 180°C – 80°C.

Figure 10 Variation of $\dot{W}_{max}$ with $[NTU/(2+NTU)]^2$: direct comparison between the sorted Pareto front solutions (open symbols) and the scaling results (solid lines) for different heat source temperatures.

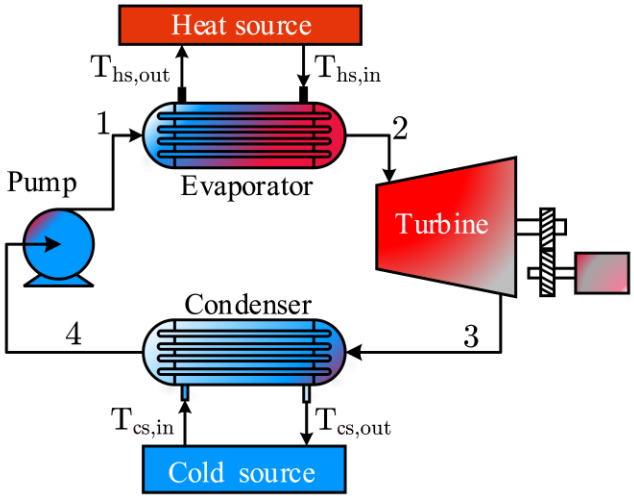
Heat source
$T_{hs,out}$
$T_{hs,in}$
1
2
Pump
Evaporator
Turbine
Condenser
4
3
$T_{cs,in}$
$T_{cs,out}$
Cold source

a)

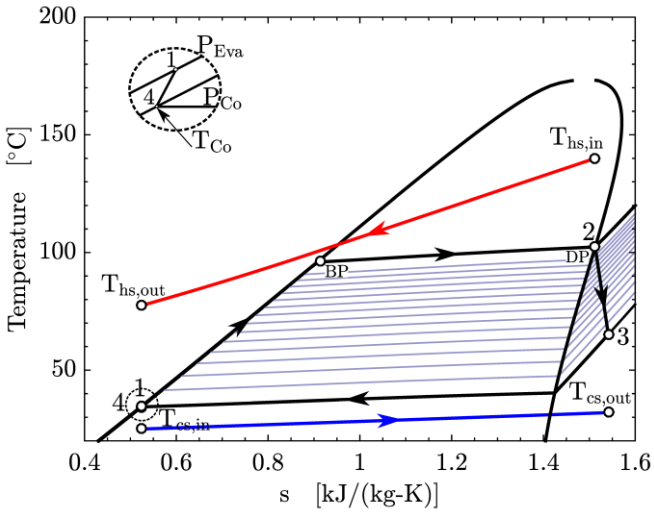
200
150
100
50
Temperature [°C]
P_{Eva}
P_{Co}
T_{Co}
1
4
$T_{hs,in}$
$T_{hs,out}$
BP
2
DP
3
$T_{cs,out}$
$T_{cs,in}$
0.4
0.6
0.8
1
1.2
1.4
1.6
s [kJ/(kg-K)]

b)

Figure 1.

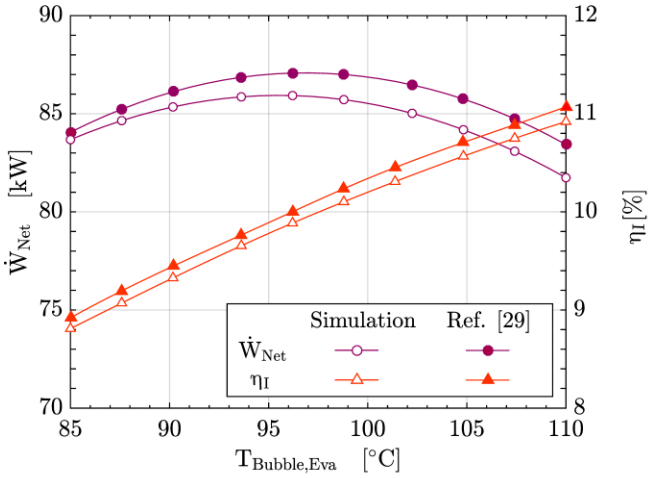
90
85
80
75
70
12
11
10
9
8
85
90
95
100
105
110
$\dot{W}_{Net}$ [kW]
η_{II} [%]
$T_{Bubble,Eva}$ [°C]
Simulation
Ref. [29]
$\dot{W}_{Net}$
η_{II}

Figure 2.

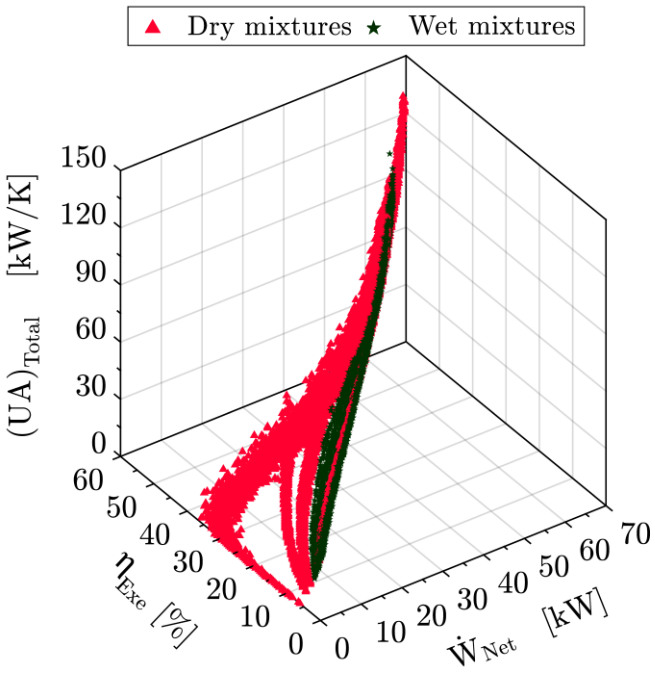
Dry mixtures
Wet mixtures
$(UA)_{Total}$ [kW/K]
150
120
90
60
30
0
60
50
40
30
20
10
0
η_{Exe} [%]
0
10
20
30
40
50
60
70
$\dot{W}_{Net}$ [kW]

Figure 3.

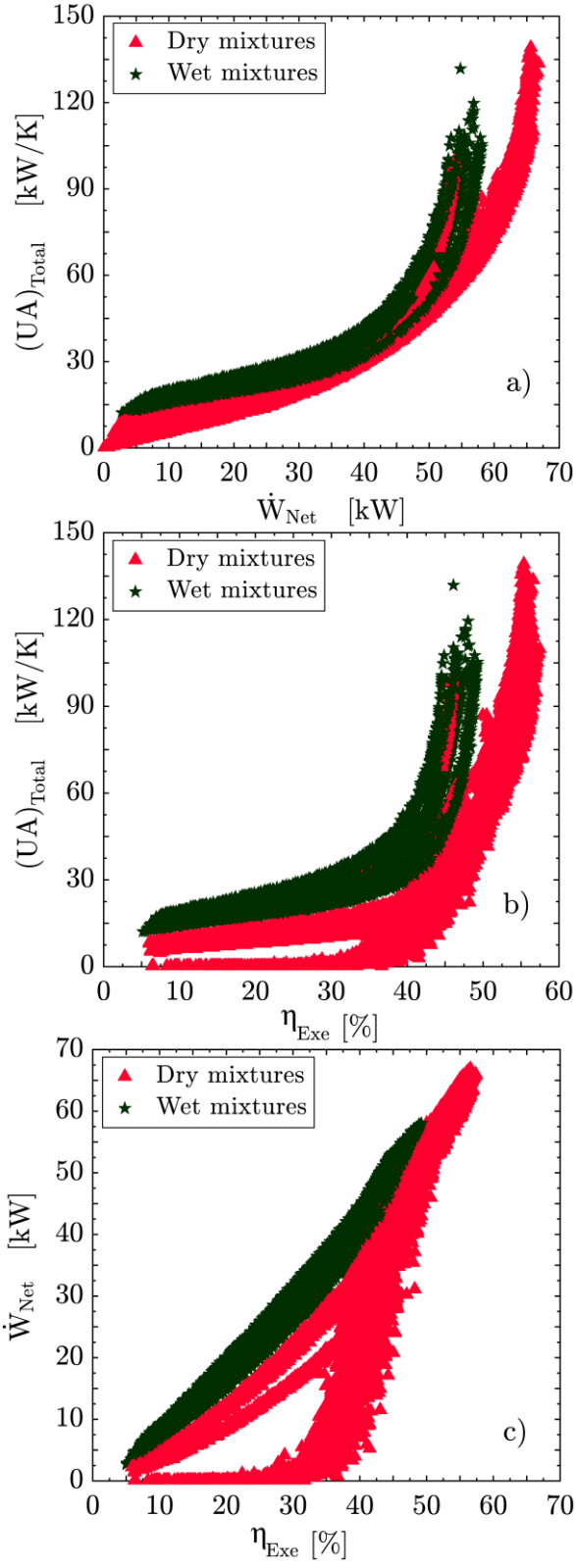
Dry mixtures
Wet mixtures
$(UA)_{Total}$ [kW/K]
$\dot{W}_{Net}$ [kW]
a)
Dry mixtures
Wet mixtures
$(UA)_{Total}$ [kW/K]
η_{Exe} [%]
b)
Dry mixtures
Wet mixtures
$\dot{W}_{Net}$ [kW]
η_{Exe} [%]
c)

Figure 4.

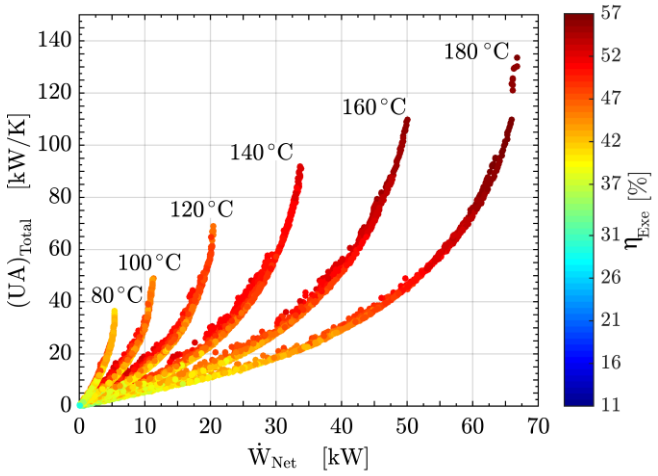
180 °C
160 °C
140 °C
120 °C
100 °C
80 °C
(UA)Total [kW/K]
Ẇ Net [kW]
ηExe [%]

(a)

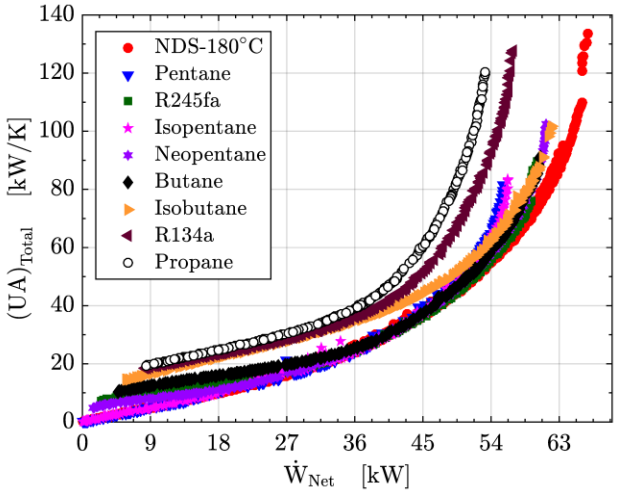
NDS-180°C
Pentane
R245fa
Isopentane
Neopentane
Butane
Isobutane
R134a
Propane
(UA)Total [kW/K]
Ẇ Net [kW]

(b)

Figure 5.

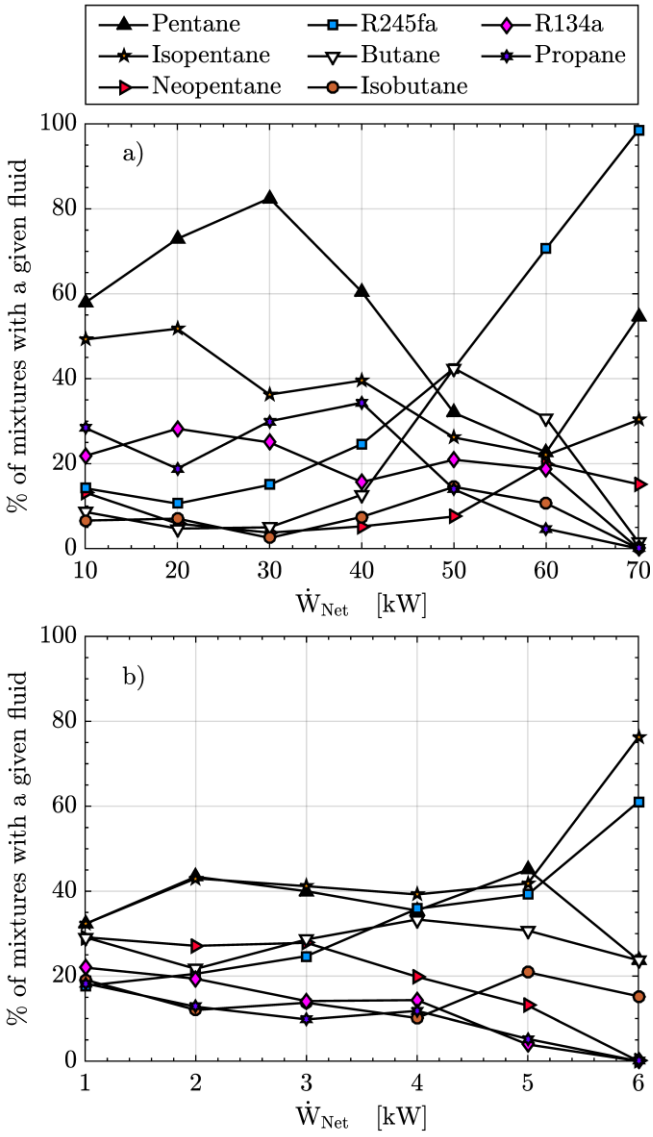
Pentane
R245fa
R134a
Isopentane
Butane
Propane
Neopentane
Isobutane
a)
b)
% of mixtures with a given fluid
$\dot{W}_{Net}$ [kW]

Figure 6.

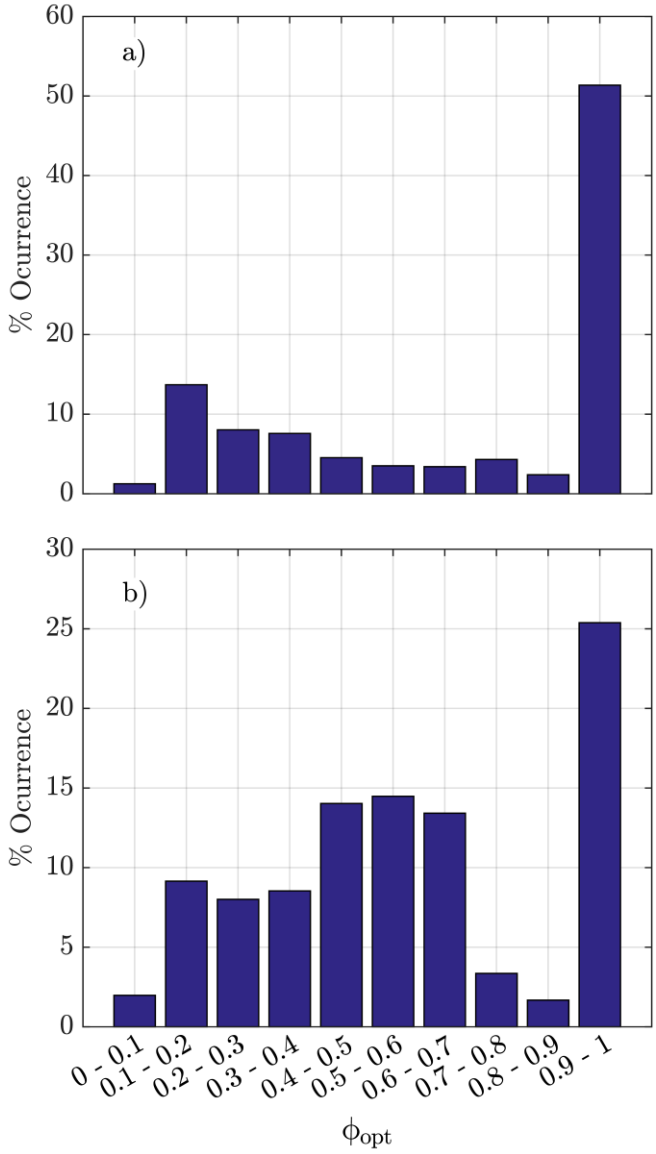
a)
% Ocurrence
60
50
40
30
20
10
0
b)
% Ocurrence
30
25
20
15
10
5
0
0 - 0.1
0.1 - 0.2
0.2 - 0.3
0.3 - 0.4
0.4 - 0.5
0.5 - 0.6
0.6 - 0.7
0.7 - 0.8
0.8 - 0.9
0.9 - 1
ϕ_{opt}

Figure 7.

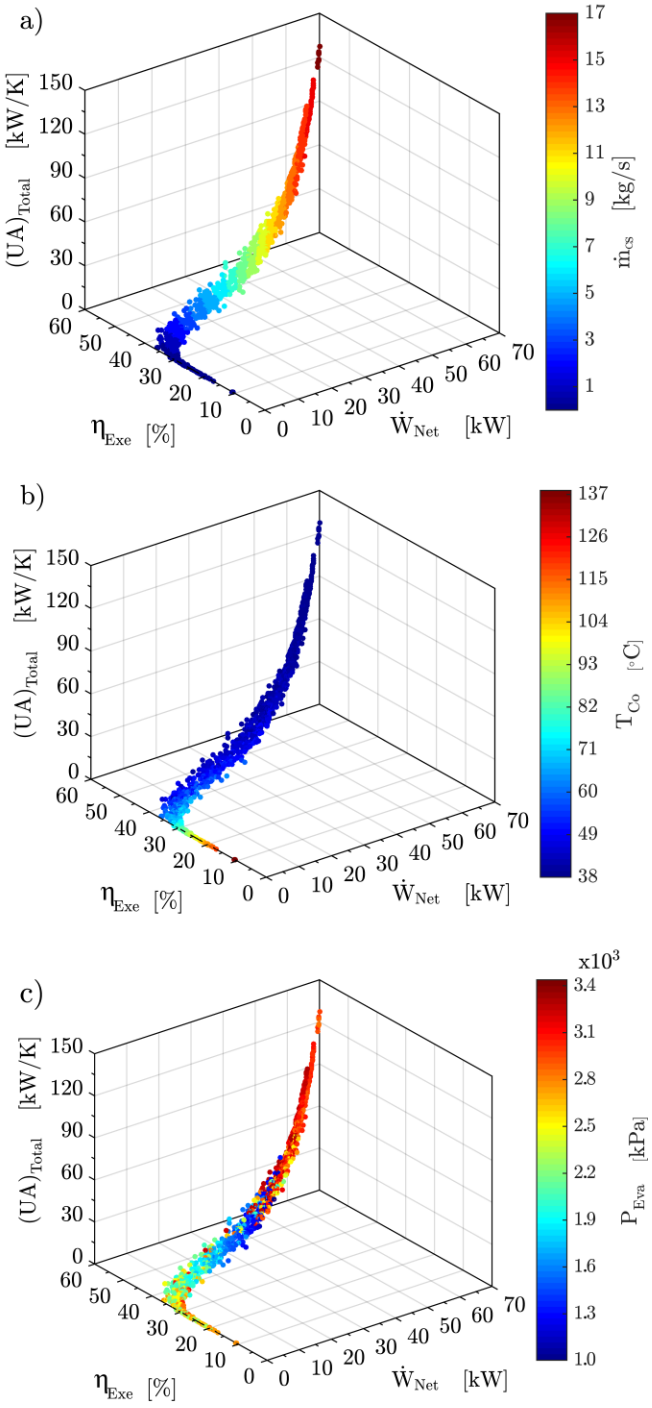
a)
$(UA)_{Total}$ [kW/K]
150
120
90
60
30
0
60
50
40
30
20
10
0
η_{Exe} [%]
0
10
20
30
40
50
60
70
$\dot{W}_{Net}$ [kW]
17
15
13
11
9
7
5
3
1
$\dot{m}_{cs}$ [kg/s]
b)
$(UA)_{Total}$ [kW/K]
150
120
90
60
30
0
60
50
40
30
20
10
0
η_{Exe} [%]
0
10
20
30
40
50
60
70
$\dot{W}_{Net}$ [kW]
137
126
115
104
93
82
71
60
49
38
T_{Co} [°C]
c)
$(UA)_{Total}$ [kW/K]
150
120
90
60
30
0
60
50
40
30
20
10
0
η_{Exe} [%]
0
10
20
30
40
50
60
70
$\dot{W}_{Net}$ [kW]
x10^3
3.4
3.1
2.8
2.5
2.2
1.9
1.6
1.3
1.0
P_{Eva} [kPa]

Figure 8.

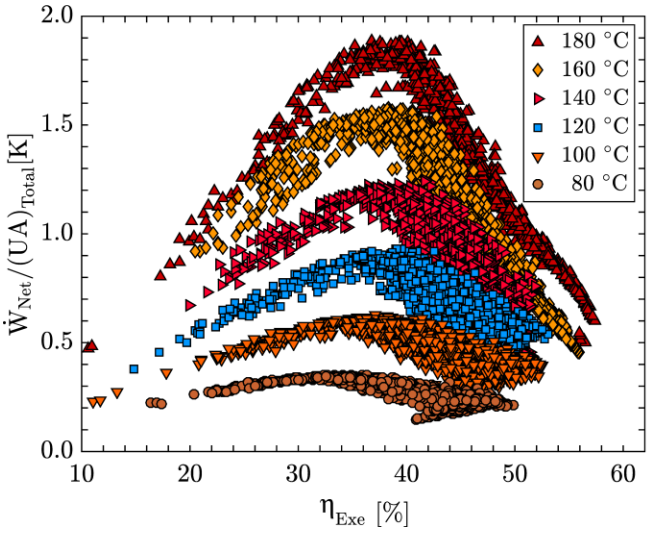
2.0
1.5
1.0
0.5
0.0
10
20
30
40
50
60
$\dot{W}_{Net,}/(UA)_{Total}$[K]
η_{Exe} [%]
180 °C
160 °C
140 °C
120 °C
100 °C
80 °C

Figure 9.

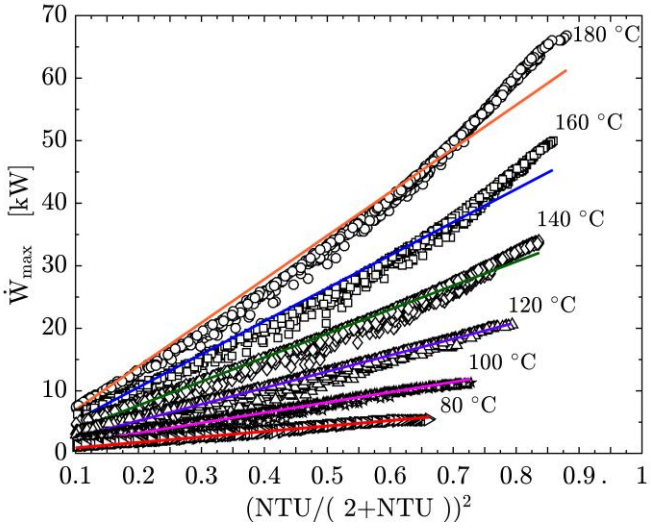
70
60
50
40
30
20
10
0
$\dot{W}_{max}$ [kW]
180 °C
160 °C
140 °C
120 °C
100 °C
80 °C
0.1
0.2
0.3
0.4
0.5
0.6
0.7
0.8
0.9
1
(NTU/(2+NTU))^2

Figure 10.